LAWRENCE
LIVERMORE
NATIONAL
LABORATORY

LLNL-JRNL-853607

Lifetime and degradation studies of poly(methylmethacrylate) via a data-driven study protocolapproach

H. H. Aung, D. Li, J. Liu, C. Barretta, Y. Sheng, Y. J. Jo, J. C. Jimenez, E. I. Barcelos, G. Oreski, R. H. French, L. S. Bruckman

August 24, 2023

Integrating Materials and Manufacturing Innovation

Integrating Materials and Manufacturing Innovation

Lifetime and Degradation Study of Poly(methyl methacrylate) via a Data-driven Study Protocol Approach

--Manuscript Draft--

Manuscript Number:	IMMJ-D-23-00105
Full Title:	Lifetime and Degradation Study of Poly(methyl methacrylate) via a Data-driven Study Protocol Approach
Article Type:	Thematic Article
Funding Information:	National Science Foundation (EEC-2052776) — Prof Laura Bruckman National Nuclear Security Administration (DE-NA0004104) — Roger H. French
Abstract:	To optimize and extend the service life of polymeric materials in outdoor environments, a domain knowledge-based and data-driven approach was utilized to quantitatively investigate the temporal evolution of degradation modes, mechanisms, and rates under various stepwise accelerated exposure conditions. Six formulations of Poly(methyl methacrylate) (PMMA) with different combinations of stabilizing additives, including one unstabilized formulation, were exposed in three accelerated weathering conditions. Degradation was dependent on wavelength as samples in UV light at 340 nm (UVA) exposure showed the most yellowing. The unstabilized PMMA formulation showed much higher yellowness index (yi) values (59.5%) than stabilized PMMA formulations (2% – 12%). Urbach edge analysis shows a shift towards longer wavelength from 285 nm to 500 nm with increasing exposure time and an increased absorbance around 400 nm of visible region as the unstabilized samples increase in yellowing. The degradation mechanisms of PMMA were tracked using induced absorbance to dose (IAD) at specific wavelengths that correspond to known degradation mechanisms. The degradation pathway of PMMA was modeled in a <Stressor|Mechanism|Response> framework using network structural equation modeling (netSEM). netSEM showed changes in degradation pathway as PMMA transition stages of degradation.
Corresponding Author:	Laura Bruckman, Ph.D. Case Western Reserve University Cleveland, OH UNITED STATES
Corresponding Author Secondary Information:	
Corresponding Author's Institution:	Case Western Reserve University
Corresponding Author's Secondary Institution:	
First Author:	Hein Htet Aung
First Author Secondary Information:	
Order of Authors:	Hein Htet Aung
	Donghui Li
	Jiqi Liu
	Chiara Barretta
	Yiyang Sheng
	Yea Jin Jo
	Jayvic Cristian Jimenez
	Erika I. Barcelos
	Gernot Oreski

	Roger H. French
	Laura Bruckman, Ph.D.
Order of Authors Secondary Information:	
Author Comments:	
Suggested Reviewers:	Michael Pecht University of Maryland pecht@umd.edu Great experience with product reliability fields and has many experience as editor in chief for multiple distinguished journals.
	Xiaohong Gu National Institute of Standards and Technology xiaohong.gu@nist.gov Dr. Gu is a Materials Research Engineer in Polymeric Materials Group at NIST and was part of groundbreaking research that linked accelerated exposure data to field performance for clear polymeric systems.

Lifetime and Degradation Study of Poly(methyl methacrylate) via a Data-driven Study Protocol Approach

Hein Htet Aung[1,2†], Donghui Li[1,3†], Jiqi Liu[1], Chiara Barretta[4], Yiyang Sheng[5], Yea Jin Jo[1], Jayvic Cristian Jimenez[6,7], Erika I. Barcelos[1,7], Gernot Oreski[4], Roger H. French[1,7,8,9], Laura S. Bruckman[1,2*]

[1]Department of Materials Science and Engineering, Case Western Reserve University, Cleveland, OH, 44106, USA.
[2]Center for Materials Data Science for Reliability and Degradation: MDS-RELY, Case Western Reserve Univeristy, Cleveland, 44106, OH, US.
[3]Pacific Northwest National Laboratory, Richland, 99354, WA, US.
[4]Polymer Competence Center Leoben GmbH, Roseggerstrasse 12, Leoben, A-8700, Austria.
[5]Department of Mathematics, Applied Mathematics and Statistics, Case Western Reserve University, Cleveland, 44106, OH, USA.
[6]Lawrence Livermore National Laboratory, Livermore, 94550 CA, USA.
[7]Materials Data Science for Stockpile Stewardship: Center of Excellence, Case Western Reserve Univeristy, Cleveland, 44106, OH, US.
[8]Department of Computer and Data Sciences, Case Western Reserve Univeristy, Cleveland, 44106, OH, US.
[9]Department of Macromolecular Science and Engineering, Case Western Reserve Univeristy, Cleveland, 44106, OH, US.

*Corresponding author(s). E-mail(s): lsh41@case.edu;
Contributing authors: hein.htetaung@case.edu; donghui.li@pnnl.gov; jxl1763@case.edu; chiara.barretta@pccl.at; ys811@georgetown.edu; yeajin.jo@case.edu; jimenez45@llnl.gov; erika.barcelos@case.edu; gernot.oreski@pccl.at; roger.french@case.edu;
†These authors contributed equally to this work.

Abstract

To optimize and extend the service life of polymeric materials in outdoor environments, a domain knowledge-based and data-driven approach was utilized to quantitatively investigate the temporal evolution of degradation modes, mechanisms, and rates under various stepwise accelerated exposure conditions. Six formulations of Poly(methyl methacrylate) (PMMA) with different combinations of stabilizing additives, including one unstabilized formulation, were exposed in three accelerated weathering conditions. Degradation was dependent on wavelength as samples in UV light at 340 nm (UVA) exposure showed the most yellowing. The unstabilized PMMA formulation showed much higher yellowness index ($\boldsymbol{yi}$) values (59.5%) than stabilized PMMA formulations (2% – 12%). Urbach edge analysis shows a shift towards longer wavelength from 285 nm to 500 nm with increasing exposure time and an increased absorbance around 400 nm of visible region as the unstabilized samples increase in yellowing. The degradation mechanisms of PMMA were tracked using induced absorbance to dose ($\boldsymbol{IAD}$) at specific wavelengths that correspond to known degradation mechanisms. The degradation pathway of PMMA was modeled in a $<\boldsymbol{Stressor}|\boldsymbol{Mechanism}|\boldsymbol{Response}>$ framework using network structural equation modeling (netSEM). netSEM showed changes in degradation pathway as PMMA transition stages of degradation.

Keywords: Polymer Degradation, PMMA, UV Absorber, HALS, Antioxidant, Optical properties

1 Introduction

Polymers are ubiquitous and have been long-standing materials given that they are cheap, easily manufactured, versatile, and most importantly, durable [1–5]. Despite all the benefits, polymers will invariably undergo degradation due to environmental or other factors directly influenced by their applications. Degradation can be described as an alteration in the physical, chemical, and/or mechanical properties of a material.

Polymer degradation can manifest from environmental stressors such as heat, electromagnetic radiation, and humidity, and from various external stressors such as chemical or mechanical factors throughout its application [6]. Exposure to sunlight, for example, leads to photooxidation of the polymer, caused by free-radicals leading to chemical changes such as chain scission, changes in the polymer's functional groups, and/or cross-linking; all of these effects can alter the polymer's intrinsic properties.

Poly(methyl methacrylate) (PMMA) was first discovered during the early 1930s. Shortly after its discovery, PMMA was found to be a promising material as a substitute for inorganic glass [7]. It is widely used, even today, because of its excellent optical properties, desirable mechanical properties, and weatherability [8–21]. Despite its versatility, however, PMMA can quickly degrade in outdoor exposures due to solar irradiation, temperature, and moisture. These factors shorten the duration and lifespan of PMMA.

Photodegradation of PMMA can be inhibited and its lifetime prolonged using chemical stabilizers such as ultraviolet (UV) absorbers [22–24], hindered amine light stabilizers (HALS) [25, 26], and antioxidants [27, 28]. These stabilizers act as sacrificial agents which are preferentially photooxidized, keeping the polymer chains chemically intact. They are often added in small quantities relative to the polymer weight, since these stabilizers act like plasticizers. They are typically incorporated within the polymer matrix during melt processing [29]. A popular example of such a class of chemical stabilizers is Tinuvin (BASF) [23]. While the incorporation of chemical preservatives helped prolong the usage of PMMA, the polymer will invariably undergo degradation at some point.

Because of PMMA's wide usage, understanding how it degrades is necessary. Fundamental studies have led to improvements such as increased durability, and literature shows progress in estimating the lifetime of PMMA [4, 5, 30–36]. Although standardized durability tests with accelerated exposures are widely used to assess failure and durability of PMMA, the results obtained are solely based on the typical pass/fail criteria, which is insufficient to describe critical features such as degradation modes, mechanisms, and kinetics. French et al. constructed a reliable study protocol for evaluating degradation and predicting the lifetime, by understanding the degradation modes and mechanisms [37].

In this study, a similar approach was performed to investigate the degradation mechanisms from weathering of PMMA. We developed a stepwise study protocol such that we can observe the synergistic effect of stressors, which are rarely investigated. Different formulations of commercial PMMA films were exposed in three different accelerated exposure conditions according to ASTM standards [38, 39]. Chemical and mechanical properties of the samples were characterized at each exposure step using non-destructive techniques including colorimetry, UV-Vis-NIR spectroscopy, optical profilometry, and micro indentation.

Insights were subsequently analyzed using a data-driven modeling technique called network structural equation modeling (netSEM). netSEM allows for exploration of variable relationships using pathway diagrams in a stressor, mechanism, and response ($<S|M|R>$) framework by describing these relationships from standard models, such as linear, quadratic, and other non-linear forms of equations [40]. The quantified relationship then describe potential degradation pathway which can be traced back to the exposure or weathering conditions that was captured during the lifetime studies [41–45]. The data-driven findings guided by domain knowledge rationalize the underlying mechanisms responsible for the PMMA degradation.

2 Methods and Materials

2.1 Poly (methyl methacrylate) Formulations

Six formulations of PMMA were investigated as summarized in Tabe 1. All the six formulations are optically clear and have a thickness of 3 mm.

Table 1 Summary of six PMMA formulation.

Brand	PMMA formulation	Description
Brand A	UVT	UV transparent. Unstabilized PMMA formulation.
	FF1	Multi-purpose. Used in security and transport industries as substrate.
	UVA	UV absorbing. Used in applications requiring extra UV protection.
Brand B	UVO	Used for general purpose.
	UVP	Used for general purpose.
	UVF	UV filtering. Used in applications requiring extra UV protection.

2.2 Accelerated Indoor Exposures

Samples were exposed to three different types of indoor accelerated conditions according to ASTM G154 and G155 standards shown in Table 2. For UV-light exposures, the QUV Accelerated Weathering Tester with fluorescent UV lamps was used to simulate the effect of critical short-wave UV in sunlight. The spectral power distribution of fluorescent UV lamps matches the AM 1.5 standard spectrum between 280 nm to 360 nm. Due to the absence of the condensing humidity cycle, the samples in Hot QUV (modified-ASTM G154 Cycle 4) has an accumulated UV dosage of 1.5 times higher than those in Cyclic QUV (ASTM G154 Cycle 4). For full spectrum light exposures, Q-SUN Xe-1/Spray was used.

Table 2 Exposure conditions of three accelerated indoor exposures based on ASTM G154 and ASTM G155 standards.

Stressor	Exposure	Condition
UV, Heat, Humidity	Cyclic QUV	Cyclic exposure of 8 hours of UVA light at 1.55 W/m^2 at 340 nm , 70°C and 4 hours of condensing humidity at 50°C in dark.
UV, heat	Hot QUV	Constant exposure of UVA light at 1.55 W/m^2 at 340 nm, 70°C.
Full Spectrum Light	QSUN	Cyclic exposure of 102 minutes of TUV light at 70W/m^2 , 63°C and 18 minutes of TUV light at 70 W/m^2, 63°C with water spray.

Stepwise exposures of twenty-four replicate samples from each of the six formulations were assigned to three different exposure types (eight samples per formulation per exposure type) so as to provide sufficient data and observations for statistical analysis. The samples were exposed for a total of 22500 hours of exposure and measured at time steps of 0 (referred to as "baseline"), 400, 800, 1200, 2200, 3200, 16200, 17400, and 22500 hours. One sample was retained at each exposure step in order to preserve the stepwise information. The retained samples are useful such that additional characterization measurements can be made in the future.

To accurately compare the xenon arc and UV light exposures, the photodose of light between 280 to 360 nm was calculated as shown in Equation 1 where UVA_{360}

is the integrated irradiance (Jm^{-2}) between 280 and 360 nm, E_λ is the irradiance (W/m^2), λ is the wavelength and t is the time under exposure.

$$UVA_{360} = \int_0^t \int_{280}^{360} E_\lambda d\lambda dt \tag{1}$$

The spectral characteristics of all three exposure conditions are shown in Table 3.

Table 3 Spectral irradiance and accumulated photodosage at end of exposure for Full spectrum, TUV, and UVA_{360}.

Calculation	Spectrum	Cyclic QUV	Hot QUV	QSUN
Irradiance (W/m^2)	Full spectrum	56.36	84.54	390.71
	TUV	56.36	84.54	70.00
	UVA	40.43	60.65	26.06
Exposure time (h)	-	22500	22500	22500
Photodose (MJ/m^2)	UVA	3275.31	4912.96	2110.99

2.3 Characterization Methods

2.3.1 Yellowness Index (yi) and Haze

Yellowness index (yi) is a qualitative determination of degradation in polymers as seen in the physical yellowing of the material. yi is a quantifiable measurement of such behavior, in accordance with ASTM E313 [46]. Haze is the ratio of diffuse transmittance to total transmittance of incident light in the wavelength range between 380 and 780 nm measured according to ASTM D1003 [47]. Herein, colorimetric measurements were performed on an UltrascanPro spectrophotometer (Hunterlab, USA) to obtain the yi and haze of the exposed samples using a D65 illuminant with viewing degree angle at 10 degrees (coefficients: $C_x = 1.3013$, $C_z = 1.1498$). The high-performance colorimeter allows fast and non-destructive measurements with a spectral range from $350 - 1050$ nm with 5 nm data output. To simulate D65 daylight, a UV attenuation filter was inserted partially in the light path of spectrophotometer. A D65 light source ensures a single standard for lighting that is applied across different products, manufacturers, and industries.

2.3.2 Gas Chromatography–Mass Spectrometry (GC-MS)

To determine the additives and stabilizers present in the PMMA samples, gas chromatography–mass spectrometry (GC-MS) was performed with a QM2010 Plus from Shimadzu with Pyrolyzer-3030D from Frontier Laboratories Ltd. The PMMA samples were heated in the pyrolyer from 60°C to 320°C at a heating rate of 20°C/min under a helium flow. The evolved gases were continuously introduced into GC and MS for identification of the substances.

2.3.3 UV-Vis-NIR

The transmittance and reflectance of the PMMA samples were measured using F10-RT (PARTS-UV) reflectometer manufactured by Filmetrics. The film coating recipe was setup as air for Medium, HC-standard-2, and Acrylic-2 for substrate.

2.3.4 Micro-Indentation

The mechanical properties of PMMA samples were investigated with Micro-Indentation test using Nanovea PB1000. Micro-Vickers testing was performed on all PMMA samples with a V2830 Indenter using different recipes for baseline samples and cracked samples. For baseline samples, a 5 N load with 10 N/min loading-unloading rate was applied with an approach speed of 30 μm. The contact load was defined at 20 mN, and creep was applied for 10 seconds with standard PID settings and Poisson's ratio set to 0.36. Five measurements at different locations on the exposed side of the samples were taken. Cracked samples were measured with the same setting as baseline samples with reduction of load to 2 N in order to avoid introducing additional cracks from micro-indentation measurements. Eight measurements were taken on the exposed side for cracked samples: four measurements near the cracked regions and four measurements at non-cracked regions. The Young's modulus and Vickers hardness values were calculated using Nanovea Mech Software.

2.3.5 Surface Roughness

Surface roughness were measured using a Zygo NewView 7300 Optical Profilometer. Images were captured with a 10 x magnification, 3 % threshold for min mod %, image resolution of 640 x 480 at 210 Hz, a scan length of 65 μm and FDA resolution was set to high 2G.

2.4 Data-driven Modeling

2.4.1 Induced Absorbance to Dose

In order to quantify degradation mechanisms and rates, IAD was calculated as a tracking metric. IAD measures the change in optical absorbance per centimeter of a sample per unit dosage [48, 49]. Average IAD allows tracking of phenomenon over large doses and is calculated as follows:

$$IAD = \frac{Abs_i(\lambda)/cm - Abs_0(\lambda)/cm}{Dose_i - Dose_0}. \quad (2)$$

where, $Dose_0$ is the dose at baseline, $Dose_i$ is the dose at time point i, $Abs_0(\lambda)/cm$ is the absorbance at baseline, and $Abs_i(\lambda)/cm$ is the absorbance at time point i. IAD is independent of thickness and is normalized over photo dosage [48], which allows comparison across samples as well as different exposure steps.

2.4.2 Urbach Parameters

Urbach parameters were obtained to evaluate the electronic structure and bonding changes in material to describe the degree of energy disorder in the polymers [50, 51].

Onsets from the UV obtained absorption spectra were fitted. The equations shown below were then used to determine the Urbach parameters based on the fitted curves,

$$A(E) = H_A exp(\frac{E - E_{0A}}{W_A}) \tag{3}$$

$$ln(A) = \frac{E - (E_{0A} - h_A W_A)}{W_A}, \tag{4}$$

where H_A and h_A are fitted parameters, and the relationship between absorbance, A, and frequency in eV, E, is characterized by the Urbach Width (W_A) and the Urbach edge energy (E_{0A})[52, 53].

2.4.3 Modeling in <*Stressor*|*Mechanism*|*Response*> Framework

An inferential model was built with netSEM using a Markovian (pairwise) process [40, 45, 54] to explore relationships between variable pairs. The **<*S*|*M*|*R*>** notation in netSEM is adapted from Dirac notation (Bra-ket notation) in quantum mechanism [55]. The adaptation in netSEM represents the pathway to ***Response*** (observation) due to a ***Mechanism*** (operator) resulting from a ***Stressor*** (operation). The strength of the relationship between variables was evaluated using adjusted R^2 and the best relationship was selected. Model equations as well as an interpretable visual pathway diagram showing the relationship between variables were also generated. PMMA degradation was explored with UV dosage as a stressor, ***IAD*** metrics as mechanistic variables to track degradation mechanisms, and yellowness index as a response.

3 Results

3.1 Detection of Additives in PMMA by GC-MS and UV-Vis

The types of additives in baseline samples of the six grades of PMMA was determined using pyrolysis GC/MS. The samples mainly contained three types of UV stabilizers: antioxidant, hindered amine light stabilizer (HALS), and UV light absorbers. The specific chemical compounds corresponding to the formulation of PMMA are shown in Table 4 and the chemical structures of the compounds are shown in Figure 1.

Table 4 Information on additives detected in baseline PMMA samples determined by GC/MS. '-' indicates that the stabilizer was undetected.

PMMA formulation	Brand	Antioxidant	HALS	UV absorber
UVT	A	-	-	-
FF1	A	-	-	Tinuvin P (possible fragment)
UVA	A	Irganox 1076	Tinvin 292	-
UVO	B	Irganox 1076	-	-
UVP	B	Irganox 1076	-	Tinuvin P, Tinuvin 327
UVF	B	Irganox 1076	-	Tinuvin P, Tinuvin 327

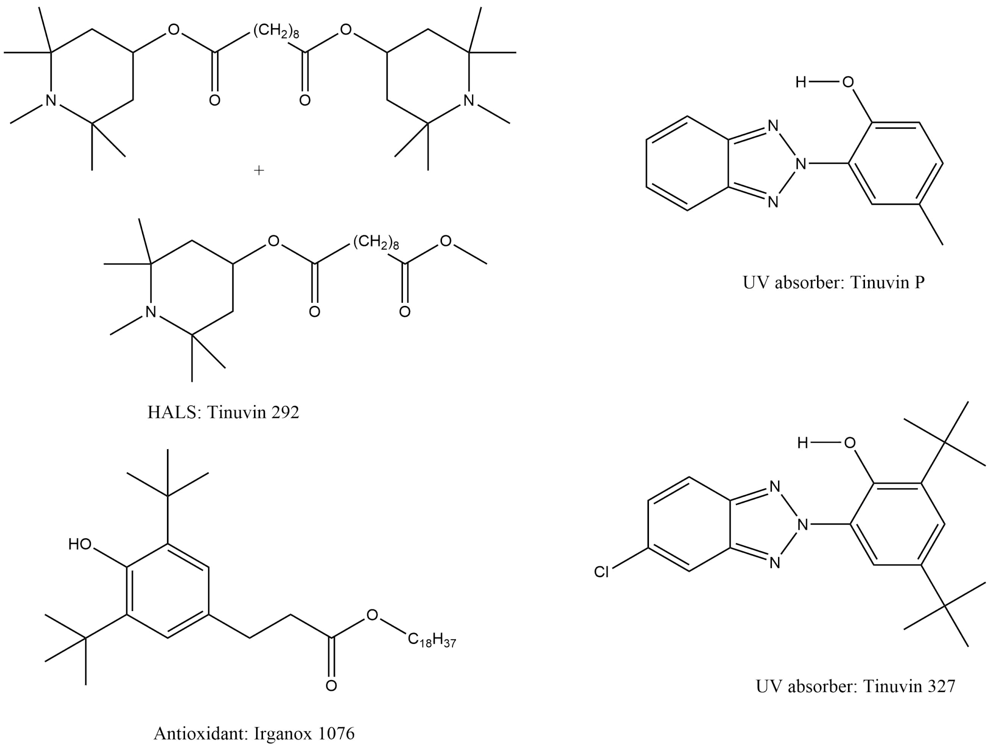

Fig. 1 Chemical structures of additives in PMMA formulations identified by GC/MS. Top Left: Tinuvin 292 (HALS), Top Right: Tinuvin P (UV absorber), Bottom Left: Irganox 1076 (Antioxidant), Bottom Right: Tinuvin 327 (UV absorber).

The hindered amine light stabilizer (HALS), Tinuvin 292, as shown in Figure 1 Top Left, is a combination of two compounds that are developed especially for coatings. Tinuvin P and Tinuvin 327, shown in Figure 1 Top Right and 1 Bottom Right, respectively, belong to a class of UV absorbers called phenolic benzotriazoles which features strong absorption between 300 nm - 400 nm with minimal absorbance in the visible range (>400 nm) providing UV protection for PMMA. Lastly, antioxidant Irganox 1076, as shown in Figure 1 Bottom Left, is a non-discoloring stabilizer that protects polymers against thermo-oxidative degradation.

The presence of additives in PMMA formulations can also be inferred from comparing the UV-Vis spectrum of baseline unstabilized UVT formulation to the remaining formulations, as shown in Figure 2. Peaks at 298 nm and 330 nm can be observed for the FF1 sample, indicating the presence of Tinuvin P. UVP and UVF, which have the same additives, as identified by GC/MS, also show the same UV-Vis spectrum. The smaller width peak around 350 nm in UVO compared to that of UVP and UVF hints the abscence of some additives that are found in UVP and UVF. The UV-Vis spectrum for UVA shows the broadest range compared to the rest of the PMMA formulation.

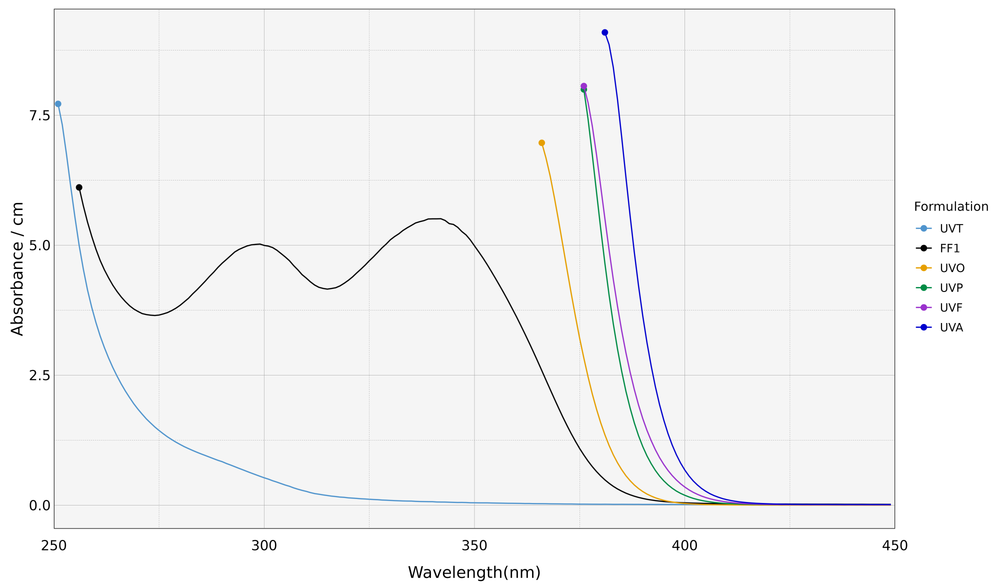

Fig. 2 The UV-Vis absorbance per cm spectrum of baseline samples for six formulations of PMMA. UVT is the unstabilized formulation. Spectrum to the left of the points are excluded due to saturation.

3.2 PMMA Samples throughout Exposure

The degradation of PMMA samples were visually observable through the exposure steps, especially for unstabilized UVT formulation. Figure 3 shows the changes in UVT samples at exposure steps 0, 5, 7, and 8 across the different exposure conditions. The gradual increase in yellowing of the samples can be observed from step 0 to step 8 for Hot QUV and Cyclic QUV exposure conditions. At step 8, cracks can be observed on samples across all exposure conditions.

3.3 Yellowness Index and Haze

The $\boldsymbol{yi}$ value was measured to assess the degree of yellowing and therefore the extent of degradation in PMMA samples under exposure. Figure 4 shows a multi-panel plot of yellowness index of PMMA with the faceting groups on the rows as three exposure types and the columns as six PMMA formulations.

Among the six formulations, the UVT samples show the highest $\boldsymbol{yi}$ values in all exposure conditions, followed by FF1 samples, compared to other PMMA formulations. Comparing across exposure conditions, samples in Hot QUV (HQUV) exposure have the highest $\boldsymbol{yi}$ values.

In addition to discoloration, PMMA degradation can also occur as loss in optical clarity, which is quantified by haze (%). Figure 5 shows the haze (%) values as a multi-panel plot with facet columns as PMMA formulations and facet rows as exposure conditions. Although there is no clear trend in haze (%) values across different PMMA

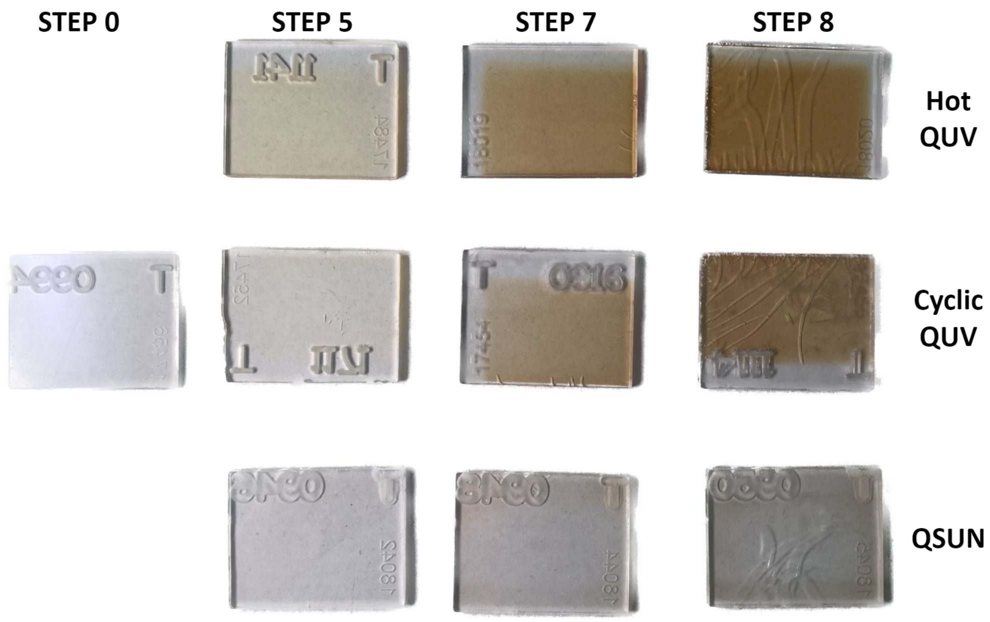

Fig. 3 Changes in UVT samples at exposure steps 0, 5 (3200 hours), 7 (17400 hours), and 8 (22500 hours) for exposure conditions Hot QUV, Cyclic QUV, and QSUN. Hot QUV contains stressors UV and Temperature. Cyclic QUV contains stressors UV, Temperature, and Humidity. QSUN contains stressors Full Spectrum Light and Humidity.

formulations, samples in QSUN show significantly higher haze (%) values compared to samples in other exposure conditions.

3.4 Induced Absorbance to Dose ($\boldsymbol{IAD}$)

The degradation mechanisms and their rates for PMMA photodegradation were evaluated with changes in $\boldsymbol{IAD}$ metrics calculated from the absorbance/cm spectrum from UV-Vis measurements. The positive $\boldsymbol{IAD}$ values indicate a photodarkening process while negative $\boldsymbol{IAD}$ values indicate a photobleaching process. Figure 6 is a multi-panel plot with exposure conditions as columns and the formulations UVT and FF1, which were formulations that showed highest $\boldsymbol{yi}$ values, as rows. $\boldsymbol{IAD}$ was tracked at specific wavelengths that correspond to known degradation mechanisms in PMMA:

- $\boldsymbol{IAD}$ at 275 nm ($\boldsymbol{IAD_{275}}$): Changes in fundamental absorption edge of PMMA.
- $\boldsymbol{IAD}$ at 298 and 339 nm ($\boldsymbol{IAD_{298}}$, $\boldsymbol{IAD_{339}}$): Photobleaching of Tinuvin P.
- $\boldsymbol{IAD}$ at 400 ($\boldsymbol{IAD_{400}}$): Formation of chromophores responsible for yellowing.

The $\boldsymbol{IAD}$ spectrum follows a consistent trend for HQUV and CQUV exposures for both UVT and FF1 formulation throughout the exposure steps. Additionally for FF1 samples, a photobleaching effect can be observed at 298 nm and 339 nm, depicted by negative $\boldsymbol{IAD}$ values. For QSUN exposure, UVT shows a photobleaching process around 300 nm, which was not observed in other exposure conditions. FF1 formulation

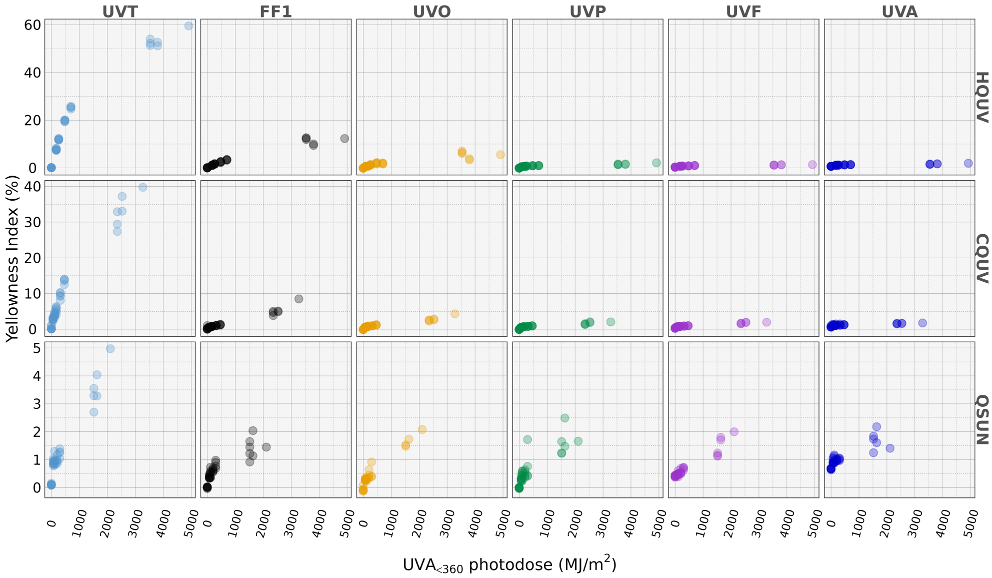

Fig. 4 Yellowness index (***yi***) plotted against photodosage of UV ¡360 nm for the six formulations of PMMA under Hot QUV (HQUV), Cyclic QUV (CQUV), and QSUN exposure. Note the scale for ***yi*** is different for each exposure condition.

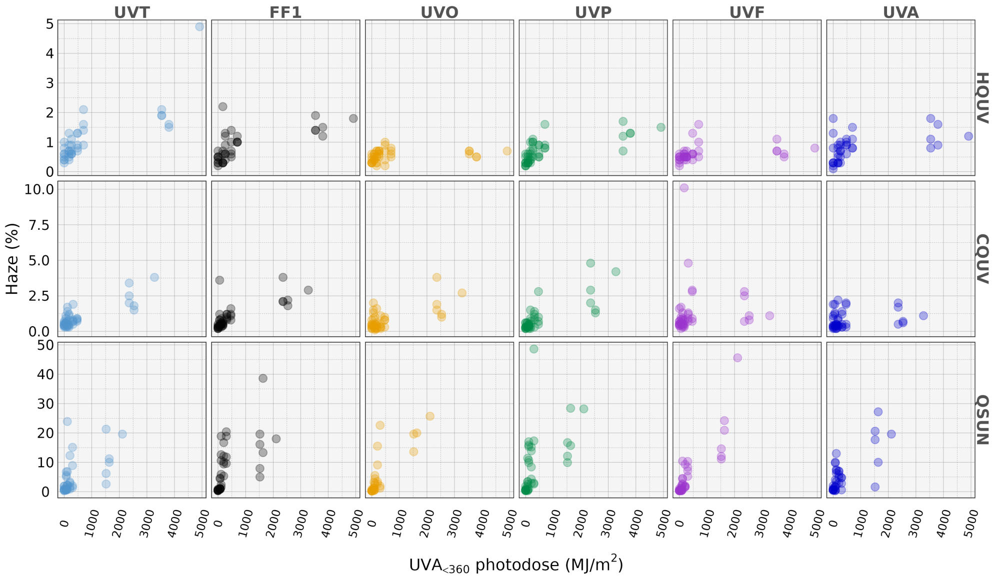

Fig. 5 Haze (%) plotted against photodosage of UV ¡360 nm for the six formulations of PMMA under Hot QUV (HQUV), Cyclic QUV (CQUV) and QSUN exposure. Note the scale for Haze (%) is different for each exposure condition.

did not have a clear trend for $\boldsymbol{IAD}$ spectrum throughout the exposure step. UVT also shows higher $\boldsymbol{IAD}$ values than FF1 formulation by approximately one magnitude.

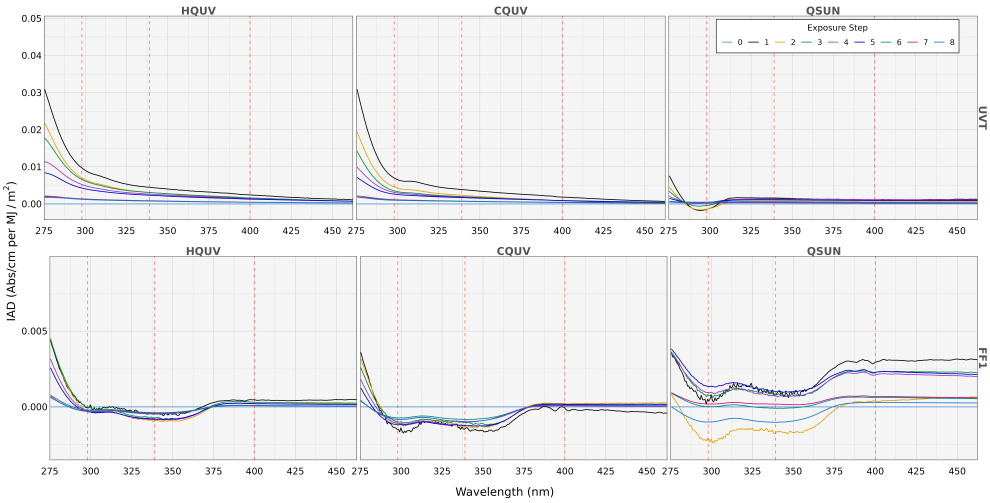

Fig. 6 Induced Absorbance to Dose value for unstabilized UVT and stabilized FF1 under exposure conditions Hot QUV (HQUV), Cyclic QUV (CQUV), and QSUN. Vertical dashed lines indicate wavelengths at 298, 339, and 400 nm.

3.5 Urbach Edge Fitting

Urbach edge fitting from the absorption spectra for all PMMA formulations prior to exposure is shown in Figure 7. The onset of UVT occurs below 300 nm while the other samples have onsets occurring above 375 nm.

Urbach edge fitting to the absorption spectra was also performed on PMMA formulations from steps 0 to 8. We focus our attention specifically at UVT and FF1, which are shown in Figure 8 and Figure 9, respectively, because there are no significant changes from the Urbach edge positions and width with the remaining PMMA formulations.

The Urbach edge positions and widths for all six PMMA formulations prior to exposure are summarized in Table 5. Formulations with additives have Urbach edges at longer wavelengths. Due to the different chemistry of the UV absorbers, the Urbach edge width varies with different formulations. UVT, which has no UV absorbers, has an Urbach edge at 285 nm.

Table 6 and Table 7 summarize the results for Urbach edge position and width for UVT and FF1 formulations in exposure, respectively. Compared to the significant shift in Urbach edge position from 285 nm - 500 nm for UVT formulation, the Urbach edge position for FF1 formulation remains around 376 nm - 378 nm.

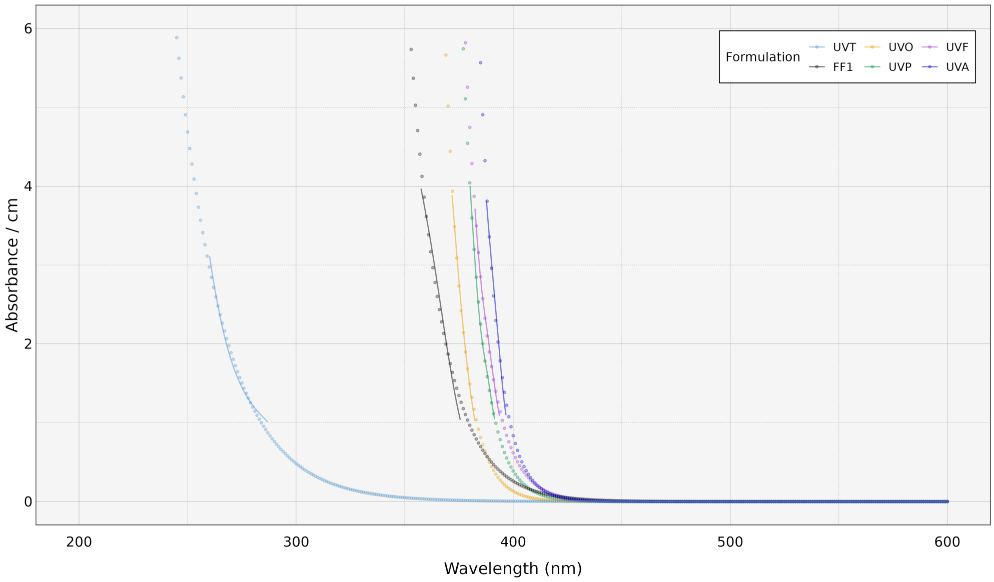

Fig. 7 Urbach fit analysis of PMMA samples prior to exposure.

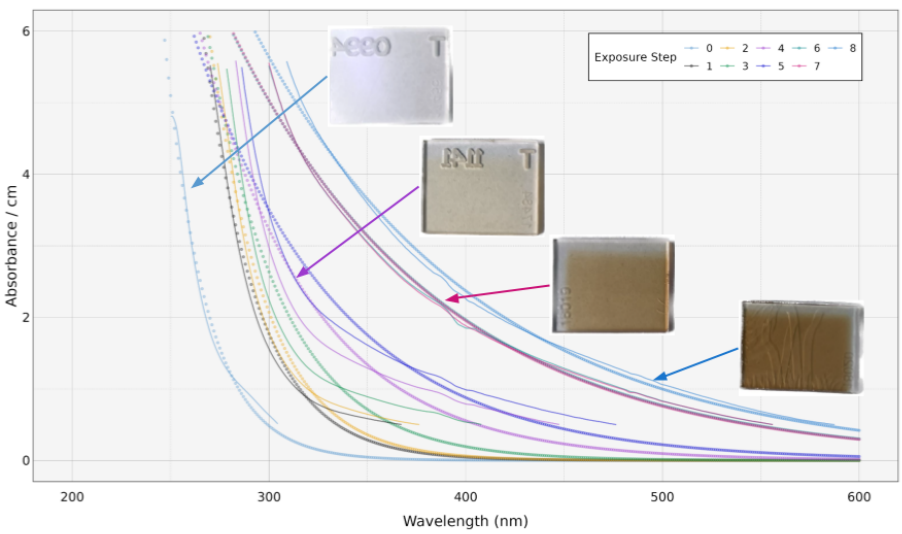

Fig. 8 The Urbach fit analysis of unstabilized UVT in Hot QUV.

3.6 <***Stressor***|***Mechanism***|***Response***> Models

After quantifying performance and exposure metrics as well as degradation mechanisms, data-driven modeling in a <***Stressor***|***Mechanism***|***Response***>

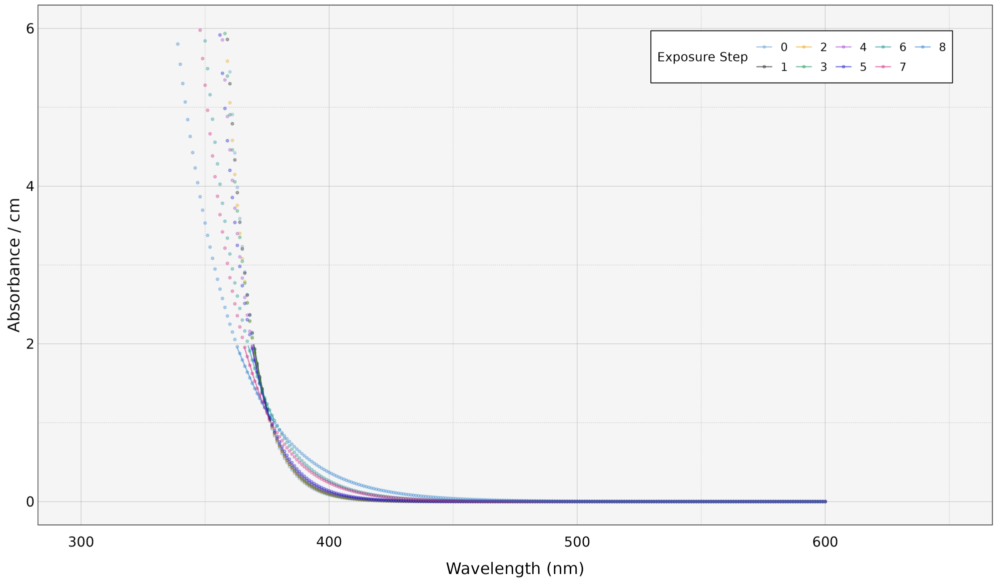

Fig. 9 The Urbach fit analysis of FF1 in Hot QUV.

Table 5 Urbach edge fit parameters for PMMA in Hot QUV at 0 hour.

PMMA formulation	Step	Exposure time (hour)	Urbach Edge position (nm)	Urbach Edge position (eV)	Urbach Edge width (eV)
UVT	0	0	285	4.35	0.40
FF1	0	0	380	3.26	0.13
UVO	0	0	383	3.24	0.07
UVP	0	0	392	3.16	0.07
UVF	0	0	395	3.14	0.08
UVA	0	0	399	3.11	0.06

Table 6 Urbach edge fit parameters for UVT PMMA in Hot QUV.

PMMA formulation	Step	Exposure time (hour)	Urbach Edge position (nm)	Urbach Edge position (eV)	Urbach Edge width (eV)
UVT	0	0	285	4.35	0.40
UVT	1	400	316	3.92	0.50
UVT	2	800	321	3.86	0.52
UVT	3	1200	337	3.68	0.67
UVT	4	2200	367	3.38	0.78
UVT	5	3200	391	3.17	0.83
UVT	6	16200	472	2.63	0.83
UVT	7	17400	471	2.63	0.82
UVT	8	22500	500	2.48	0.81

($<\boldsymbol{S}|\boldsymbol{M}|\boldsymbol{R}>$) framework using the netSEM-markovian model was performed to understand and explore the degradation pathways of PMMA. In the context of

Table 7 Urbach edge fit parameters for FF1 PMMA in Hot QUV.

PMMA formulation	Step	Exposure time (hour)	Urbach Edge position (nm)	Urbach Edge position (eV)	Urbach Edge width (eV)
FF1	0	0	376	3.30	0.08
FF1	1	400	377	3.29	0.09
FF1	2	800	376	3.30	0.09
FF1	3	1200	377	3.29	0.09
FF1	4	2200	377	3.29	0.10
FF1	5	3200	377	3.29	0.10
FF1	6	16200	378	3.28	0.14
FF1	7	17400	377	3.29	0.14
FF1	8	22500	378	3.28	0.20

the $<\boldsymbol{S}|\boldsymbol{M}|\boldsymbol{R}>$ framework, UV dosage was defined as a stressor, $\boldsymbol{IAD}$ values as mechanistic variables, and $\boldsymbol{yi}$ as response.

The degradation of PMMA was modeled in three different phases corresponding to the changes observed at exposure steps 5, 7, and 8. netSEM-markovian models the relationship between each variable pair with linear and non-linear forms of equations and returns the best fit equation by determining the highest adjusted R^2. The results for unstabilized UVT and stabilized FF1 samples in Hot QUV samples are shown in particular because Hot QUV exposure conditions induce much higher $\boldsymbol{yi}$ values compared to other exposure conditions. UVT and FF1 samples result in a much higher yellowing compared to the rest of the PMMA formulations.

Figure 10 shows the degradation pathway diagram generated from the netSEM-markovian model for UVT samples in Hot QUV exposure for three phases of degradation. The relationship between UV dose ($\boldsymbol{uvdose}$) and yellowness index ($\boldsymbol{yi}$) depicts the $<\boldsymbol{Stressor}|\boldsymbol{Response}>$ ($<\boldsymbol{S}|\boldsymbol{R}>$) relationship, which transitions from a change point behavior in Phase 1 to a quadratic behavior in Phase 2 and reverting back to a change point in Phase 3. Throughout the different phases, the adjusted R^2 values remain significantly high, inferring a very good correlation between $\boldsymbol{uvdose}$ and $\boldsymbol{yi}$. There is a high correlation in the relationship of $\boldsymbol{IAD_{400}}$ with $\boldsymbol{uvdose}$ and $\boldsymbol{yi}$ across all three phases.

Interestingly, $\boldsymbol{IAD_{275}}$, which is related to the Fundamental Absorption Edge of PMMA, only has high correlation during Phase 1 for the relationships with $\boldsymbol{uvdose}$ and $\boldsymbol{yi}$, trickling down to a low adjusted R^2 value for Phases 2 and 3.

Similarly, the degradation pathway of FF1 samples can also be explored, as shown in Figure 11. The difference between the degradation pathway for FF1 and UVT is the consideration of $\boldsymbol{IAD_{298}}$ and $\boldsymbol{IAD_{339}}$ in the degradation modeling, as FF1 contains Tinuvin P as a stabilizer. The relationship between UV dose and $\boldsymbol{yi}$ has a high correlation across all three phases. The relationship between $\boldsymbol{IAD_{400}}$ and $\boldsymbol{yi}$ disappeared after Phase 1 and the relationship between $\boldsymbol{IAD_{275}}$ and $\boldsymbol{yi}$ disappeared in Phase 2.

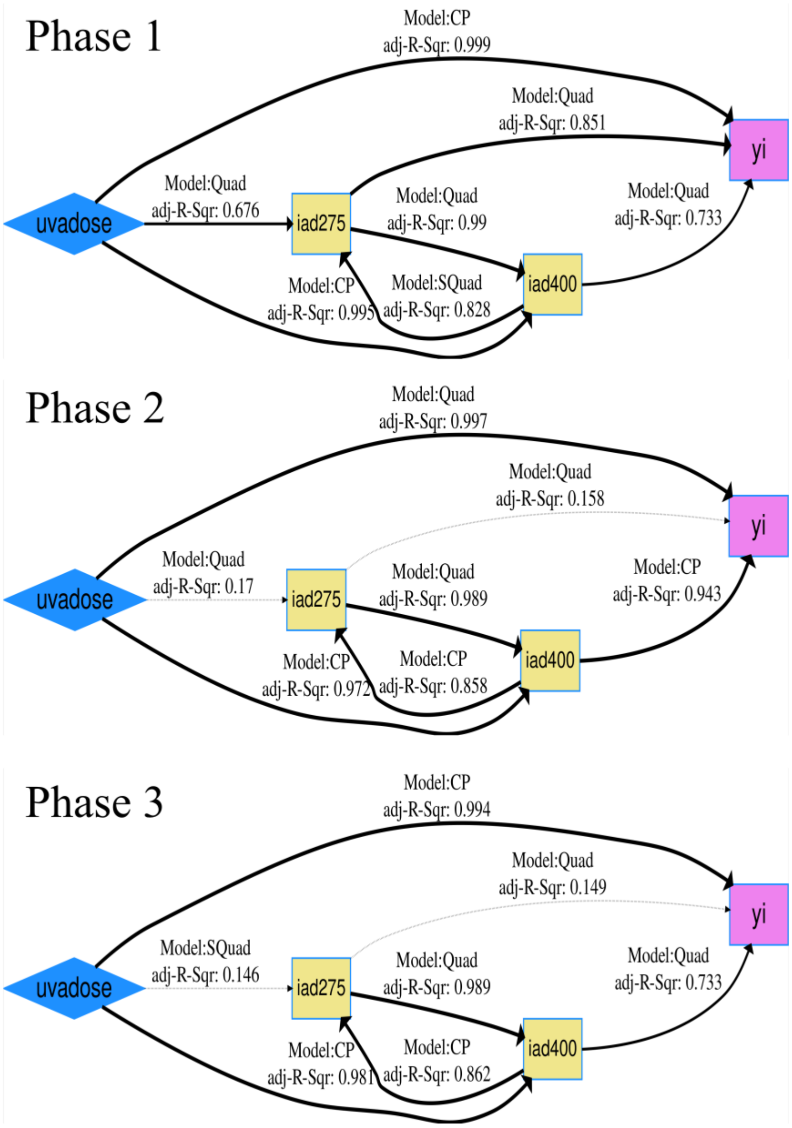

Fig. 10 Comparison of Phases in Acrylic Degradation for unstabilized UVT samples using Inferential (Markovian) Model from netSEM. CP indicates change point model. Quad indicates Quadratic model. Phase 1 is modeled using data from step 0 - 5. Phase 2 is modeled using data from step 0 - 7. Phase 3 is modeled using data from step 0 - 8.

3.7 Mechanical Characterization

3.7.1 Surface Roughness

The surface roughness of samples exposed in QSUN was initially investigated using optical profilometry for samples at exposure steps 0, 3, and 5 in QSUN exposure due to the high haze (%) formation observed in step 5 samples. The haze formation

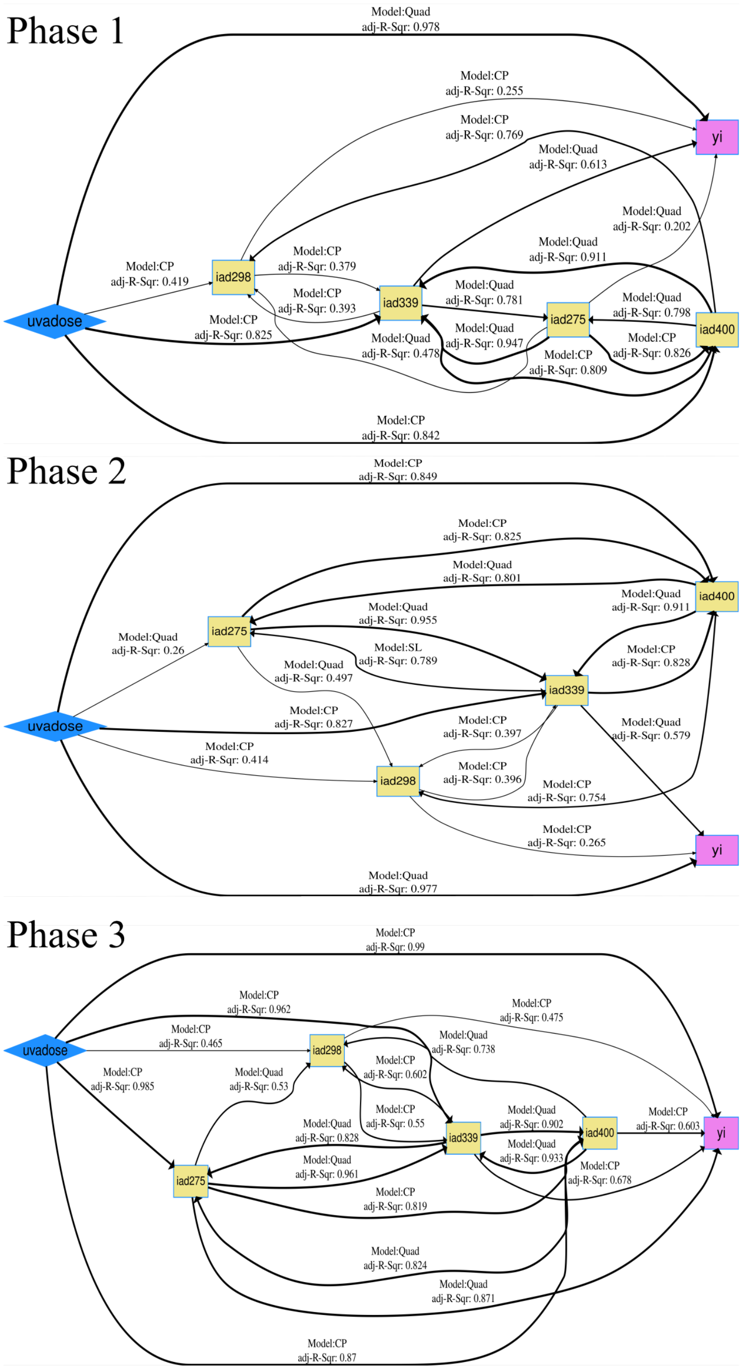

Fig. 11 Comparison of Phases in Acrylic Degradation for stabilized FF1 samples using Inferential (Markovian) Model from netSEM. CP indicates change point model. Quad indicates Quadratic model. Phase 1 is modeled using data from step 0 - 5. Phase 2 is modeled using data from step 0 - 7. Phase 3 is modeled using data from step 0 - 8.

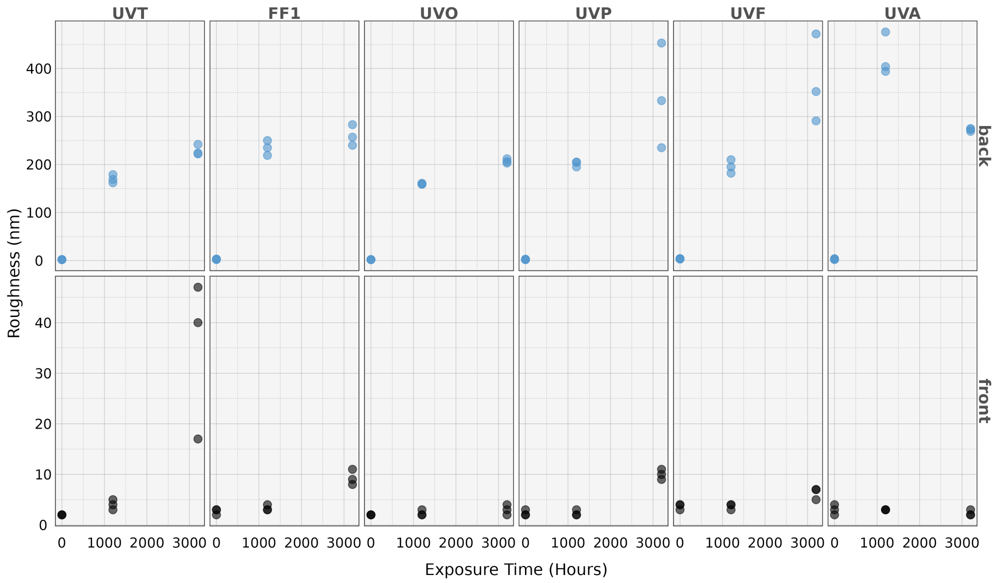

Fig. 12 Surface roughness of irradiated side (front) and non-irradiated side (back) in QSUN.

in samples was observed as an opaque spot in the center of the backside of sample with the haze value (%) of the spot increasing with the increasing irradiance dosage, resulting in a visually observable spot by step 5 exposure. The roughness of the back side of the samples was observed to be higher than the irradiated front side, as shown in Figure 12.

3.7.2 Micro Indentation

Cracks visually observed in the step 8 exposure were evaluated using micro-indentation. The effect of different exposure conditions on the mechanical properties of unstabilized UVT and stabilized FF1 samples for baseline 0 and 8 exposure steps were assessed by measurements of stiffness and surface hardness of the sample using Young's Modulus and Vickers Hardness.

As illustrated in Figures 13 and 14, a higher Young's Modulus and Vickers Hardness was observed for baseline stabilized FF1 formulations comparatively to unstabilized baseline UVT samples. Comparing between the two exposure steps, samples at step 8 for both FF1 and UVT formulations show a statistically significant decrease in Young's Modulus, with the exception of HQUV exposure condition for UVT samples. In addition, a larger decrease in Young's Modulus for FF1 samples compared to that of UVT samples can be observed in Cyclic QUV (CQUV) and Hot QUV (HQUV). Nevertheless, FF1 samples in QSUN exposure still maintain higher Young's Modulus values than UVT samples. There was also no statistically significant difference between Young's Modulus values for CQUV and HQUV exposure conditions for both step 8 UVT and FF1 formulations.

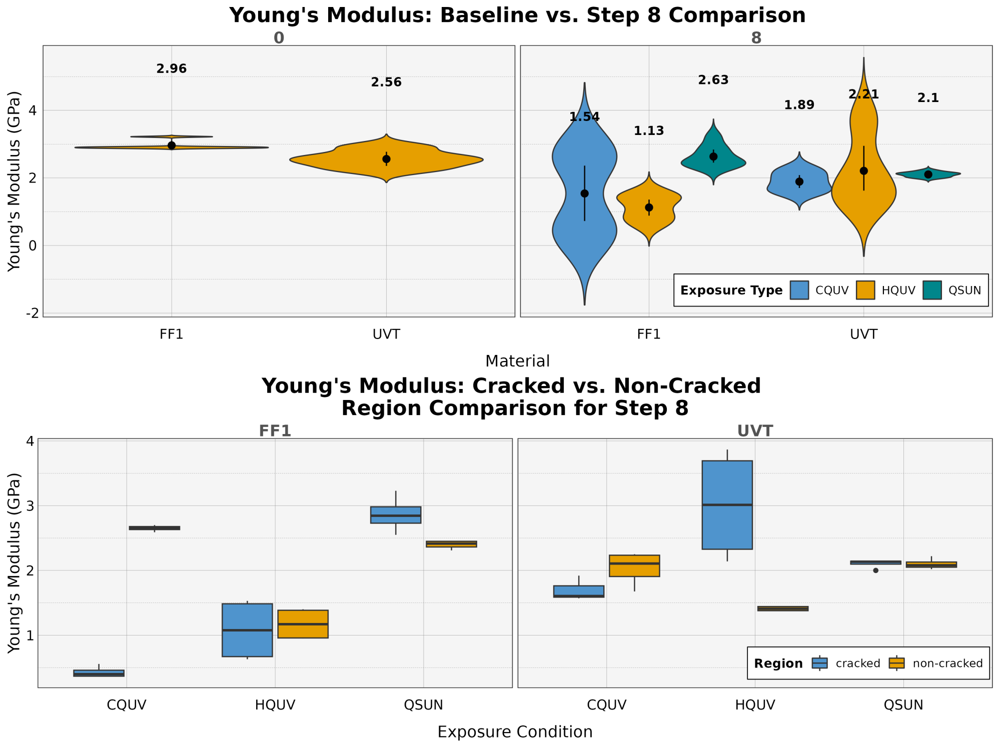

Fig. 13 *Top*: Comparison of Young's Modulus between baseline (Step 0) and step 8 samples for unstabilized UVT and stabilized FF1 formulations. Error bars indicate 83.4 % confidence interval. *Bottom*: Comparison of Young's Modulus between cracked and non-cracked region of sample for step 8 exposure for different exposure conditions: HQUV, CQUV, and QSUN.

For Vickers Hardness, all step 8 samples for FF1 formulation show a statistically significant decrease for all exposure conditions, while there was no difference for samples with UVT formulation. There was also no statistically significant difference in Vickers Hardness between HQUV and CQUV exposure conditions for FF1 and UVT samples in step 8. However, FF1 samples have lower values of Vickers Hardness than that of UVT samples in HQUV exposure, but are more or less the same for CQUV and QSUN exposure conditions.

A comparison for cracked and non-cracked regions for step 8 samples do not show a trend across different exposure conditions, except that the mechanical properties in each sample are not homogeneous, as seen in Figure 13 and 14.

4 Discussion

4.1 Acrylic Degradation Study Protocol

A study protocol involving the exposure of PMMA formulations to different exposure conditions with a varying combination of known degradation stressors allow us to

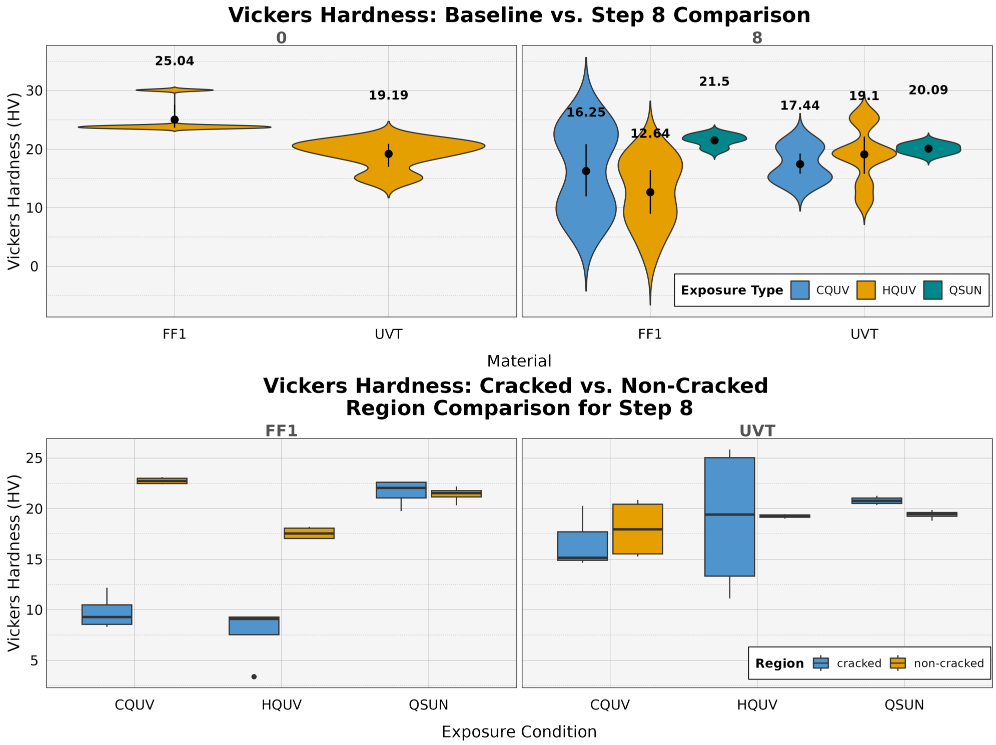

Fig. 14 *Top*: Comparison of Surface Hardness (Vickers Hardness) between baseline (step 0) and step 8 samples for unstabilized UVT and stabilized FF1 formulations. Error bars indicate 83.4% confidence interval. *Bottom*: Comparison of Surface Hardness (Vickers Hardness) between cracked and non-cracked region of sample for step 8 exposure for different exposure conditions: HQUV, CQUV, QSUN.

study the synergistic affect as well as the isolated contribution of degradation from stressors. The rate of degradation can be compared for UV and Full Spectrum Light Exposure or the presence of moisture. In addition, investigating varying combinations of PMMA formulations — with one unstabilized formulation set as a control — allows to understand the impact of protective additives on the rate of degradation. A stepwise exposure and evaluation provides higher resolution to track changes in samples that could otherwise be overlooked in a holistic exposure evaluated at the final exposure step. More importantly, the retained samples allow the addition of characterization methods during the investigation period.

4.2 Effect of Exposures on Degradation of PMMA Chemical Properties

Discoloration or yellowing is one of the main performance losses in PMMA occurring from the photodegradation. PMMA can undergo photooxidation caused by free-radical formation induced by UV. The methylmethacrylate is converted into a peroxyl radical species, which can impact the polymer backbone structure [5, 56–58].

Samples exposed in Hot QUV exposure had a much higher ***yi*** compared to samples in other exposures. This is because Hot QUV has the largest amount of accumulated UVA-340 dosage compared to other exposure conditions. In addition, the synergistic effect of temperature and UV irradiation may also account for the highest yellowing rate observed in the highly intensified exposure in Hot QUV. Additionally, photolytic degradation of PMMA occurs around wavelengths 300 nm - 330 nm due to the absorbance from ester groups and potentially carbonyl groups [5]. This explains why samples have the lowest ***yi*** values in QSUN exposure which uses full spectrum light. Thermal degradation in PMMA gains significance at temperatures above 150°C [30]. Since the temperature for exposure conditions is around 70°C, thermal degradation is less apparent compared to photolytic degradation.

The rate of degradation can also be observed in the ***IAD*** spectrum. Unstabilized UVT samples, which have higher ***yi*** values than FF1 samples, also have much higher ***IAD*** values. In FF1 samples, the negative ***IAD*** values around 298 and 339 nm show the bleaching of Tinuvin P UV absorber as the samples go through degradation. This shows that Tinuvin P is being sacrificed in order to the protect the sample from degradation.

We also observed that the Urbach edge position for UVT samples shift towards a longer wavelength as it goes through degradation. The shift is due to the formation of degradation by-products in the polymer matrix [59]. The Urbach edge position is also related to the yellowing of the sample for UVT formulation, as shown in Figure 8. The sample gets more yellow as the absorbance increases in the visible wavelength region around 400 nm, which indicates that blue light is being absorbed. Compared to UVT, FF1 formulations, which contain additives, barely shift in Urbach edge position. This suggests that the role of the light stabilizers prevent degradation, therefore mitigating changes in PMMA's optical properties.

4.3 Effect of Exposures on Degradation of PMMA Mechanical Properties

4.3.1 Investigation of Haze Formation

Surface roughness of samples exposed in QSUN exposure were evaluated to investigate the haze formation at the back side of the samples. The changes in surface roughness for samples from steps 0 to 5 in QSUN exposure is most likely related to interaction between the residual water from QSUN water spray cycle and the backside of PMMA samples. The residual water on the backside cannot totally evaporate during the 102-minute full spectrum light-only exposure cycle in QSUN, which means that the center of backside of samples in QSUN is in contact with water all the time during the 3200 hours of exposure. That fact can explain why there are more haze formations in the center of the backside of PMMA sample in QSUN compared to samples in other exposure conditions. Consequently, it can be inferred that the combination of moisture and full-spectrum light exposure with the inability for water to evaporate are the main stress conditions that lead to the significant haze formation as opposed to the combination of moisture and UV exposure.

4.3.2 Investigation of Crack Formation

The Young's Modulus and Surface Hardness were evaluated using micro indentation to investigate the conditions behind crack formation in PMMA samples.

Samples from baseline (step 0) and step 8 exposures were measured to compare the changes in mechanical properties, as cracks were visually observed on the samples by step 8 exposure. UVT unstabilized and FF1 stabilized samples were measured in particular to investigate the presence of additives on the degradation of mechanical properties, especially since these samples showed the highest degree of cracking compared to other PMMA formulations.

A higher Young's Modulus (stiffer) and surface hardness values found in baseline FF1 samples (step 0) in comparison to UVT samples could be attributed to the presence of additives in FF1 samples. As the samples undergo degradation after being exposed to different exposure conditions, a decrease in Young's Modulus and Vickers Hardness is observed, especially for FF1 samples in Hot QUV and Cyclic QUV exposure conditions.

Chain scission has shown to be the main mechanism of photodegradation in PMMA, which could potentially explain the reduction in Young's Modulus of the samples as polymer chains get broken up, which reduces the stiffness of the polymer matrix [60]. In addition to the UV initiated chain scission mechanism, the presence of moisture can further enhance the reduction in Young's Modulus. Water molecules can be attracted by hydrophillic groups of the polymer chain and act as a plasticizer, which increases the free volume between polymer chains, thus making the polymer matrix less stiff and causing a reduction in Young's Modulus [61, 62].

However, unlike what was observed in [60] with increasing surface hardness with decreasing molecular weight, we observed a decreasing surface hardness of the PMMA samples. The decrease in surface hardness could be due to water molecules acting as a plasticizer, especially in a Cyclic QUV exposure condition, which contains a condensing humidity cycle. Samples in QSUN exposure, which are exposed to full spectrum light and water spray, do not show much reduction in Young's Modulus and surface hardness. This infers the importance of UV as the main stress factor to the degradation of PMMA samples. It is interesting to observe that FF1 samples presented greater decrease in Young's Modulus and surface hardness compared to UVT samples, as it was expected that stabilized FF1 samples would be less degraded than unstabilized UVT samples.

4.4 Degradation Pathway Models of PMMA

The netSEM-markovian model on different subsets of the exposure steps of PMMA samples shows changes in behavior of relationship between variables as well as the strength of the relationship (changes in adjusted R^2). The three different phases observed visually in the samples as well as modeled using the netSEM-markovian model could indicate the three different phases of degradation in PMMA [37]:

- Stage 1: Bleaching of UV stabilizers.
- Stage 2: Breaking of Acrylic backbone structure.
- Stage 3: Degradation of mechanical Properties.

The changes in netSEM-markovian degradation pathway diagrams were more apparent in the case of FF1 samples. As we moved from Phase 1 to Phase 3, we observed that $\boldsymbol{IAD_{275}}$ and $\boldsymbol{IAD_{400}}$ — which are mechanistic variables to track the changes in Fundamental Absorption Edge of PMMA and formation of chromophores for yellowing, respectively — start to lose significance in their relationship to yellowness index. $\boldsymbol{IAD_{298}}$ and $\boldsymbol{IAD_{339}}$, which are variables to track changes in Tinuvin P, were shown to be more correlated in their relationship with UV dose as well as yellowness index.

5 Conclusion

A domain knowledge-based and data-driven approach was utilized to quantitatively investigate the temporal evolution of degradation modes, mechanisms, and rates under various stepwise exposure conditions in PMMA. The impact of additives and different exposure conditions on the degradation of PMMA was investigated using a study protocol involving six formulations of PMMA with different combinations of UV additives exposed under three weathering conditions with various combinations of stress factors.

Evaluation of yellowness index as a performance metric highlighted the performance of additives as the unstabilized samples showed much higher $\boldsymbol{yi}$ values compared to stabilized samples. UVA-340 was also found to be more damaging to PMMA samples than full spectrum light regardless of the presence of moisture inferring the wavelength dependency in the degradation process. A shift in Urbach edge towards longer wavelengths was found to be consistent with the degradation of samples, as the absorbance around 400 nm wavelength increases with the increase in yellowing of samples. The use of Induced Absorbance to Dose to track degradation mechanisms allowed the comparison of degradation rates across different PMMA formulations and exposure conditions.

netSEM modeling showed the transition in the degradation phases of PMMA, which was also visibly observed as the samples eventually increase in yellowing and begin to crack. This informs the consideration of temporal change of mechanical properties during degradation for future studies, which could be conducted using the retained samples. The degradation pathway diagram with netSEM also allows inference for which degradation mechanism could take precedence over others from the strength of adjusted R^2 between relationships in a $<\boldsymbol{Stressor}|\boldsymbol{Mechanism}|\boldsymbol{Response}>$ framework. A degradation science study protocol approach, along with degradation modeling informed by a $<\boldsymbol{Stressor}|\boldsymbol{Mechanism}|\boldsymbol{Response}>$ framework, is a useful tool for exploring and understanding degradation mechanisms in a weathering study.

Acknowledgments

Research was performed at the SDLE Research Center, which was established through funding by the Ohio Third Frontier, Wright Project Program Award tech 12-004. This work made use of the Rider High Performance Computing Resource in the Core Facility for Advanced Research Computing at Case Western Reserve University. Microindentation measurements were performed at the CWRU Materials for Opto/electronics

Research and Education (MORE) Center, a CWRU core facility est. 2011 via Ohio Third Frontier grant TECH 09-021.

This material is based upon work supported by the U.S. National Science Foundation Award EEC-2052776 and EEC-2052662 in the MDS-Rely IUCRC Center, under the NSF Solicitation: NSF 20-570 Industry-University Cooperative Research Centers Program (*H.H.A, L.S.B*). This material is based upon research in the Materials Data Science for Stockpile Stewardship Center of Excellence (MDS3-COE), and supported by the Department of Energy's National Nuclear Security Administration under Award Number(s) DE-NA0004104 (*R.H.F* and *J.C.J*). This work was performed, in part, under the auspices of the U.S. Department of Energy by Lawrence Livermore National Laboratory under Contract DE-AC52-07NA27344, LLNL-JRNL-853607-DRAFT (*J.C.J*).

Abridged Legal Disclaimer

The views expressed herein do not necessarily represent the views of the U.S. Department of Energy or the United States Government.

Conflict of Interests

On behalf of all authors, the corresponding author states that there is no conflict of interest.

References

[1] Hsinjin Edwin Yang, Roger H. French, Laura S. Bruckman (eds.): Durability and Reliability of Polymers and Other Materials in Photovoltaic Modules, 1st edition edn. Elsevier, William Andrew Applied Science Publishers, Amsterdam (2019). https://doi.org/10.1016/C2016-0-01032-X

[2] Campo, E.A.: Industrial Polymers - Hanser Publications, (2007). https://www.hanserpublications.com/Products/150-industrial-polymers.aspx Accessed 2020-01-16

[3] Kurr, F.: Handbook of Plastics Failure Analysis (eBook) - Hanser Publications, (2015). https://www.hanserpublications.com/Products/360-handbook-of-plastics-failure-analysis-ebook.aspx Accessed 2020-03-04

[4] Gupta, A., Liang, R., Tsay, F.D., Moacanin, J.: Characterization of a Dissociative Excited State in the Solid State: Photochemistry of Poly(methyl methacrylate). Photochemical Processes in Polymeric Systems. 5. Macromolecules **13**(6), 1696–1700 (1980-11-01) https://doi.org/10.1021/ma60078a060 . Accessed 2020-02-07

[5] Dickens, B., Martin, J.W., Waksman, D.: Thermal and photolytic degradation of plates of poly(methyl methacrylate) containing monomer. Polymer **25**(5), 706–715 (1984-05-01) https://doi.org/10.1016/0032-3861(84)90041-7 . Accessed 2020-02-07

[6] Allen, N.S.: Fundamentals of Polymer Degradation and Stabilisation / Norman S. Allen and Michele Edge. Elsevier Applied Science, London ; New York (1992)

[7] Ali, U., Karim, K.J.B.A., Buang, N.A.: A Review of the Properties and Applications of Poly (Methyl Methacrylate) (PMMA). Polymer Reviews **55**(4), 678–705 (2015-10-02) https://doi.org/10.1080/15583724.2015.1031377 . Accessed 2020-02-07

[8] D4802, A.: ASTM D4802 - 10 Standard Specification for Poly(Methyl Methacrylate) Acrylic Plastic Sheet

[9] Harper, C.A.: Modern Plastics Handbook, 1st edition edn. McGraw-Hill Education, New York (2000). https://www.accessengineeringlibrary.com/content/book/9780070267145

[10] Frazer, R.Q., Byron, R.T., Osborne, P.B., West, K.P.: PMMA: An Essential Material in Medicine and Dentistry. Journal of Long-term Effects of Medical Implants (2005-01-01) https://doi.org/10.1615/JLongTermEffMedImplants.v15.i6.60 . Accessed 2020-03-04

[11] Koh, Y., Jang, S., Kim, J., Kim, S., Ko, Y.C., Cho, S., Sohn, H.: DBR PSi/PMMA composite materials for smart patch application. Colloids and Surfaces A: Physicochemical and Engineering Aspects **313-314**, 328–331 (2008-02-01) https://doi.org/10.1016/j.colsurfa.2007.04.103 . Accessed 2020-01-16

[12] Chakraborty, H., Sinha, A., Mukherjee, N., Ray, D., Protim Chattopadhyay, P.: A study on nanoindentation and tribological behaviour of multifunctional ZnO/PMMA nanocomposite. Materials Letters **93**, 137–140 (2013-02-15) https://doi.org/10.1016/j.matlet.2012.11.075 . Accessed 2020-01-16

[13] Thomas, P., Ernest Ravindran, R.S., Varma, K.B.R.: Structural, thermal and electrical properties of poly(methyl methacrylate)/CaCu3Ti4O12 composite sheets fabricated via melt mixing. Journal of Thermal Analysis and Calorimetry **115**(2), 1311–1319 (2014-02) https://doi.org/10.1007/s10973-013-3500-x . Accessed 2020-01-16

[14] Wu, H., Ma, G., Xia, Y.: Experimental study of tensile properties of PMMA at intermediate strain rate. Materials Letters **58**(29), 3681–3685 (2004-11-01) https://doi.org/10.1016/j.matlet.2004.07.022 . Accessed 2020-01-16

[15] El-Bashir, S.M., Al-Harbi, F.F., Elburaih, H., Al-Faifi, F., Yahia, I.S.: Red photoluminescent PMMA nanohybrid films for modifying the spectral distribution of solar radiation inside greenhouses. Renewable Energy **85**, 928–938 (2016-01-01) https://doi.org/10.1016/j.renene.2015.07.031 . Accessed 2020-03-04

[16] Hammam, M., El-Mansy, M.K., El-Bashir, S.M., El-Shaarawy, M.G.: Performance

evaluation of thin-film solar concentrators for greenhouse applications. Desalination **209**(1), 244–250 (2007-04-30) https://doi.org/10.1016/j.desal.2007.04.034 . Accessed 2020-03-04

[17] Yang, L., Zhou, S., Wu, L.: Preparation of waterborne self-cleaning nanocomposite coatings based on TiO2/PMMA latex. Progress in Organic Coatings **85**, 208–215 (2015-08-01) https://doi.org/10.1016/j.porgcoat.2015.04.012 . Accessed 2020-03-04

[18] Bora, M.Ö.: The influence of heat treatment on scratch behavior of polymethylmethacrylate (PMMA). Tribology International **Complete**(78), 75–83 (2014) https://doi.org/10.1016/j.triboint.2014.04.030 . Accessed 2020-03-04

[19] Hamouda, A.M.S.: The influence of humidity on the deformation and fracture behaviour of PMMA. Journal of Materials Processing Technology **124**(1), 238–243 (2002-06-10) https://doi.org/10.1016/S0924-0136(02)00096-1 . Accessed 2020-03-04

[20] Jaiganesh, V., christopher, A., Mugilan, E.: Manufacturing of PMMA Cam Shaft by Rapid Prototyping. Procedia Engineering **97**, 2127–2135 (2014-01-01) https://doi.org/10.1016/j.proeng.2014.12.456 . Accessed 2020-03-04

[21] Moghbelli, E., Banyay, R., Sue, H.-J.: Effect of moisture exposure on scratch resistance of PMMA. Tribology International **69**, 46–51 (2014-01-01) https://doi.org/10.1016/j.triboint.2013.08.012 . Accessed 2020-03-04

[22] Arndt, T., Richter, S., Pasierb, M.: Accelerated laboratory weathering of acrylic lens materials. AIP Conference Proceedings **1556**(1), 218–221 (2013-09-27) https://doi.org/10.1063/1.4822235 . Accessed 2020-03-08

[23] Pickett, J.E., Moore, J.E.: Photodegradation of UV screeners. Polymer Degradation and Stability **42**(3), 231–244 (1993-01-01) https://doi.org/10.1016/0141-3910(93)90219-9 . Accessed 2020-03-08

[24] Pickett, J.E., Moore, J.E.: Photostability of UV Screeners in Polymers and Coatings. In: Polymer Durability. Advances in Chemistry, vol. 249, pp. 287–301. American Chemical Society, ??? (1996-05-05). https://doi.org/10.1021/ba-1996-0249.ch019 . https://doi.org/10.1021/ba-1996-0249.ch019 Accessed 2020-03-08

[25] Hamid, S.H.: Handbook of Polymer Degradation, 2nd edn. CRC Press, Boca Raton (2014). https://doi.org/10.1201/9781482270181

[26] Gerlock, J.L., Smith, C.A., Núñez, E.M., Cooper, V.A., Liscombe, P., Cummings, D.R., Dusibiber, T.G.: Measurements of Chemical Change Rates to Select Superior Automotive Clearcoats. In: Polymer Durability. Advances in Chemistry, vol. 249, pp. 335–347. American Chemical Society, ??? (1996-05-05). https://doi.org/10.1021/ba-1996-0249.ch022 . https://doi.org/10.1021/ba-1996-0249.ch022

Accessed 2020-03-08

[27] Chang, T.C., Yu, P.Y., Hong, Y.S., Wu, T.R., Chiu, Y.S.: Effect of phenolic phosphite antioxidant on the thermo-oxidative degradation of PMMA. Polymer Degradation and Stability **77**(1), 29–34 (2002-01-01) https://doi.org/10.1016/S0141-3910(02)00076-9 . Accessed 2020-03-08

[28] Troitskii, B.B., Troitskaya, L.S., Yakhnov, A.S., Dmitriev, A.A., Anikina, L.I., Denisova, V.N., Novikova, M.A.: Temperature Limit of Inhibition of Thermo-oxidative Degradation of Polystyrene and Poly(methyl methacrylate) by Antioxidants. International Journal of Polymeric Materials and Polymeric Biomaterials **46**(1-2), 315–330 (2000-06-01) https://doi.org/10.1080/00914030008054864 . Accessed 2020-03-08

[29] Vlachopoulos, J., Strutt, D.: Polymer processing. Materials Science and Technology **19**(9), 1161–1169 (2003) https://doi.org/10.1179/026708303225004738

[30] Fox, R.B., Isaacs, L.G., Stokes, S.: Photolytic degradation of poly(methyl methacrylate). Journal of Polymer Science Part A: General Papers **1**(3), 1079–1086 (1963-03-01) https://doi.org/10.1002/pol.1963.100010321 . Accessed 2018-12-03

[31] Semen, J., Lando, J.B.: The Acid Hydrolysis of Isotactic and Syndiotactic Poly(methyl methacrylate). Macromolecules **2**(6), 570–575 (1969-11-01) https://doi.org/10.1021/ma60012a003 . Accessed 2020-02-07

[32] Hirata, T., Kashiwagi, T., Brown, J.E.: Thermal and oxidative degradation of poly(methyl methacrylate): Weight loss. Macromolecules **18**(7), 1410–1418 (1985-07-01) https://doi.org/10.1021/ma00149a010 . Accessed 2020-02-07

[33] Kashiwagi, T., Hirata, T., Brown, J.E.: Thermal and oxidative degradation of poly(methyl methacrylate) molecular weight. Macromolecules **18**(2), 131–138 (1985-02-01) https://doi.org/10.1021/ma00144a003 . Accessed 2019-11-16

[34] Manring, L.E.: Thermal degradation of poly(methyl methacrylate). 4. Random side-group scission. Macromolecules **24**(11), 3304–3309 (1991-05-01) https://doi.org/10.1021/ma00011a040 . Accessed 2020-02-07

[35] Torikai, A., Hattori, T., Eguchi, T.: Wavelength effect on the photoinduced reaction of polymethylmethacrylate. Journal of Polymer Science Part A: Polymer Chemistry **33**(11), 1867–1871 (1995-08) https://doi.org/10.1002/pola.1995.080331114 . Accessed 2014-12-02

[36] Kaczmarek, H., Kamińska, A., Herk, A.: Photooxidative degradation of poly(alkyl methacrylate)s. European Polymer Journal **36**(4), 767–777 (2000-04-01) https://doi.org/10.1016/S0014-3057(99)00125-1 . Accessed 2020-02-07

[37] French, R.H., Podgornik, R., Peshek, T.J., Bruckman, L.S., Xu, Y., Wheeler, N.R., Gok, A., Hu, Y., Hossain, M.A., Gordon, D.A., Zhao, P., Sun, J., Zhang, G.-Q.: Degradation science: Mesoscopic evolution and temporal analytics of photovoltaic energy materials. Current Opinion in Solid State and Materials Science **19**(4), 212–226 (2015) https://doi.org/10.1016/j.cossms.2014.12.008 . Accessed 2015-11-19

[38] Committee, A.G.: ASTM G154-23: Standard Practice for Operating Fluorescent Ultraviolet (UV) Lamp Apparatus for Exposure of Materials vol. ASTM G154-23, (2023). https://doi.org/10.1520/G0154-23

[39] Committe, A.: ASTM G155-23: Standard Practice for Operating Xenon Arc Lamp Apparatus for Exposure of Materials vol. ASTM G155-23, (2023). https://doi.org/10.1520/G0155-21

[40] Venkat, S.N., Yu, X., Liu, J., Wegmueller, J., Jimenez, J.C., Barcelos, E.I., Aung, H.H., Li, X., Jaubert, J.-N., French, R.H., Bruckman, L.S.: Statistical analysis and degradation pathway modeling of photovoltaic minimodules with varied packaging strategies. Frontiers in Energy Research **11** (2023) https://doi.org/10.3389/fenrg.2023.1127796

[41] Gok, A., Fagerholm, C.L., French, R.H., Bruckman, L.S.: Temporal evolution and pathway models of poly(ethylene-terephthalate) degradation under multi-factor accelerated weathering exposures. PLoS ONE **14**(2) (2019-02-15) https://doi.org/10.1371/journal.pone.0212258 30768646. Accessed 2020-03-07

[42] Murray, M.P., Bruckman, L.S., French, R.H.: Photodegradation in a stress and response framework: poly(methyl methacrylate) for solar mirrors and lens. J. Photon. Energy **2**(1), 022004–022004 (2012) https://doi.org/10.1117/1.JPE.2.022004

[43] Wheeler, N.R., Bruckman, L.S., Ma, J., Wang, E., Wang, C.K., Chou, I., Sun, J., French, R.H.: Statistical and domain analytics for informed study protocols. In: 2013 IEEE Energytech, pp. 1–7 (2013). https://doi.org/10.1109/EnergyTech.2013.6645354

[44] Wheeler, N.R., Gok, A., Peshek, T.J., Bruckman, L.S., Goel, N., Zabiyaka, D., Fagerholm, C.L., Dang, T., Alcantara, C., Terry, M.L., French, R.H.: A data science approach to understanding photovoltaic module degradation. In: Reliability of Photovoltaic Cells, Modules, Components, and Systems VIII, vol. 9563, p. 95630. International Society for Optics and Photonics, ??? (2015). https://doi.org/10.1117/12.2209204

[45] Bruckman, L.S., Wheeler, N.R., Ma, J., Wang, E., Wang, C.K., Chou, I., Sun, J., French, R.H.: Statistical and Domain Analytics Applied to PV Module Lifetime and Degradation Science. IEEE Access **1**, 384–403 (2013) https://doi.org/10.1109/ACCESS.2013.2267611

[46] Committee, A.E.: ASTM E313: Standard Practice for Calculating Yellowness and Whiteness Indices from Instrumentally Measured Color Coordinates, (2020). DOI: 10.1520/E0313-20

[47] Committee, A.D.: ASTM D1003: Standard Test Method for Haze and Luminous Transmittance of Transparent Plastics, (2021). DOI:10.1520/D1003-21

[48] French, R.H., Tran, H.V.: Immersion Lithography: Photomask and Wafer-Level Materials. Annual Review of Materials Research **39**(1), 93–126 (2009) https://doi.org/10.1146/annurev-matsci-082908-145350

[49] Murray, M.P., Bruckman, L.S., French, R.H.: Durability of Materials in a Stress-Response Framework: Acrylic Materials for Photovoltaic Systems. In: MRS Online Proceedings Library Archive, vol. 1391 (2012/ed). https://doi.org/10.1557/opl.2012.1241

[50] Kronemeijer, A.J., Pecunia, V., Venkateshvaran, D., Nikolka, M., Sadhanala, A., Moriarty, J., Szumilo, M., Sirringhaus, H.: Two-Dimensional Carrier Distribution in Top-Gate Polymer Field-Effect Transistors: Correlation between Width of Density of Localized States and Urbach Energy. Advanced Materials **26**(5), 728–733 (2014) https://doi.org/10.1002/adma.201303060

[51] The electronic density of states. In: Street, R.A. (ed.) Hydrogenated Amorphous Silicon. Cambridge Solid State Science Series, pp. 62–94. Cambridge University Press, Cambridge (1991). https://doi.org/10.1017/CBO9780511525247.004

[52] Yang, M.K., French, R.H., Tokarsky, E.W.: Optical properties of Teflon® AF amorphous fluoropolymers. Journal of Micro/Nanolithography, MEMS, and MOEMS **7**(3), 033010 (2008-07) https://doi.org/10.1117/1.2965541 . Accessed 2020-02-13

[53] Bahgat, A.A., El-Samanoudy, M.M., Sabry, A.I.: Optical and electrical properties of binary WO3–Pb3O4 glasses. Journal of Physics and Chemistry of Solids **60**(12), 1921–1931 (1999-12-01) https://doi.org/10.1016/S0022-3697(99)00211-5 . Accessed 2020-02-13

[54] Huang, W.-H., Wheeler, N., Klinke, A., Xu, Y., Du, W., Verma, A.K., Gok, A., Gordon, D., Wang, Y., Liu, J., Curran, A., Fada, J., Ma, X., Braid, J., Carter, J., Bruckman, L., French, R.: netSEM: Network Structural Equation Modeling. The Comprehensive R Archive Network (2018)

[55] Dirac, P.A.M.: A New Notation for Quantum Mechanics. Mathematical Proceedings of the Cambridge Philosophical Society **35**(3), 416–418 (1939) https://doi.org/10.1017/S0305004100021162

[56] Martin, J.W., Dickens, B., Waksman, D., Bentz, D.P., Byrd, W.E., Embree, E., Roberts, W.E.: Thermal degradation of poly(methyl methacrylate) at 50°C to

125°C. Journal of Applied Polymer Science **34**(1), 377–393 (1987) https://doi.org/10.1002/app.1987.070340130 . Accessed 2020-02-09

[57] Shlyapintokh, V.Y., Gol'Denberg, V.I.: Effect of photostabilizers on the rate of photodegradation of polymethylmethacrylate. European Polymer Journal **10**(8), 679–684 (1974-08-01) https://doi.org/10.1016/0014-3057(74)90179-7 . Accessed 2020-02-09

[58] Bowden, M.J., Chandross, E.A., Kaminow, I.P.: Mechanism of refractive index increase in photosensitized poly(methyl methacrylate). Polymer Engineering & Science **14**(7), 494–497 (1974) https://doi.org/10.1002/pen.760140706 . Accessed 2020-02-09

[59] Rashidian, M., Dorranian, D.: Low-intensity uv effects on optical constants of pmma film. Journal of Theoretical and Applied Physics **8**(2), 121 (2014) https://doi.org/10.1007/s40094-014-0121-0 . Citation Key Alias: rashidianLow-intensityUVEffects2014

[60] Babo, S., Ferreira, J.L., Ramos, A.M., Micheluz, A., Pamplona, M., Casimiro, M.H., Ferreira, L.M., Melo, M.J.: Characterization and long-term stability of historical pmma: Impact of additives and acrylic sheet industrial production processes. Polymers **12**(1010), 2198 (2020) https://doi.org/10.3390/polym12102198

[61] Kaddouri, A., Serier, B., Kaddouri, K., Belhouari, M.: Experimental analysis of the physical degradation of polymers – the case of polymethyl methacrylate. Frattura ed Integrità Strutturale **14**(5353), 66–80 (2020) https://doi.org/10.3221/IGF-ESIS.53.06

[62] Bokoi, Y., Ishiyama, C., Shimojo, M., Shiraishi, Y., Higo, Y.: Effects of sorbed water on crack propagation in poly(methyl methacrylate) under static tensile stress. Journal of Materials Science **35**(19), 5001–5011 (2000) https://doi.org/10.1023/A:1004803030131


17454
18019

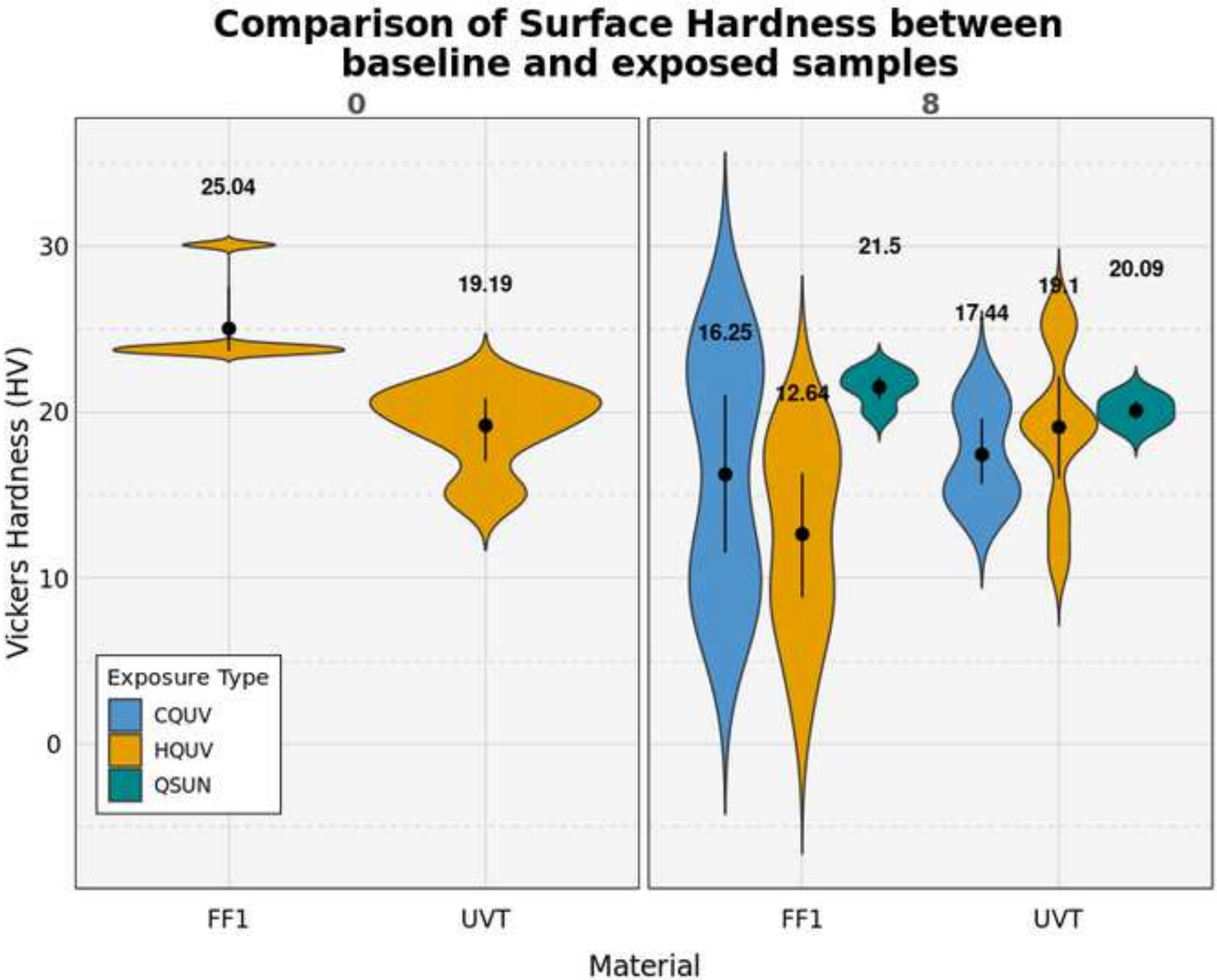
Comparison of Surface Hardness between baseline and exposed samples
0
8
25.04
19.19
16.25
12.64
21.5
17.44
19.1
20.09
30
20
10
0
Vickers Hardness (HV)
Exposure Type
CQUV
HQUV
QSUN
FF1
UVT
FF1
UVT
Material

Click here to access/download
Supplementary Material
2308Bruckman-LetterHead-netSEM-Acrylic.pdf